Original article

Coupling mechanisms of displacement and imbibition in pore-fracture system of tight oil reservoir

Zhiyang Pi[1], Huanhuan Peng[2], Zhihao Jia[1], Jinchong Zhou[1], Renyi Cao[1]*

[1]*College of Petroleum Engineering, China University of Petroleum, Beijing 102249, P. R. China*
[2]*Research Institute of Petroleum Exploration and Production, Petrochina, Beijing 100083, P. R. China*

Abstract:
Fracturing and water flooding have been popular technologies to achieve the effective development of tight oil reservoirs in recent years. However, in the late stage of production, the oil recovery rate declines with a rapid increase in the water cut. Water huff-puff could improve reservoir energy; however, the displacement and imbibition in the micro-nano pore throat and fracture systems are complex processes with unclear characteristics and position. Therefore, it is urgent to study the coupling mechanisms of oil-water displacement and imbibition in tight oil reservoirs. In this work, based on the phase field method of COMSOL Multiphysics software, we establish a two-dimensional microscopic numerical simulation model of the pore-fracture system, and carry out displacement-imbibition simulation programs of different injection media (water and surfactant) and injection methods (displacement, displacement-imbibition). By comparing the saturations and pressure distributions of different simulation programs, we analyze the changes in the oil-water interface, and summarize the action conditions of counter-current imbibition and pore throat limit. Finally, reasonable development suggestions are proposed for tight oil reservoirs.

1. Introduction

China has abundant reserves of tight oil reservoirs, with resources about three times as large of conventional oil and gas, as well as huge development potential. They are are concentrated in the Ordos, Songliao, Junggar and Qaidam basins (Zou et al., 2018). Tight oil reservoirs have received great research interest in the field of global oil and gas development due to their extremely low permeability, small pore throat size and poor reservoir properties (Cai et al.,2021, Zhou et al., 2022). The idea of conventional development is stimulated reservoir volume (SRV) to form a complex fracture network system in a large area near the wellbore. On the one hand, conventional water injection easily leads to water channeling; on the other hand, the contact area between matrix and fracture is greatly increased, and the imbibition of oil and water is significantly strengthened (Habibi et al., 2015).

Therefore, it is of great importance to study the coupling mechanisms of displacement and imbibition during huff and puff in tight oil reservoirs (Ghanbari and Dehghanpour, 2016).

Imbibition is a natural physical phenomenon, which refers to one fluid displacing another fluid in porous media by capillary pressure (Rose, 1961; Abd et al., 2019). It is also called capillary rise or capillary filling effect, which plays increasingly important roles in the chemical, hydrology, environment, and petroleum engineering fields (Alava et al., 2004; Abbasi et al., 2018; Meng et al., 2019; Liu and Sheng, 2020), especially in fractured tight oil reservoirs. Various methods exist for studying the imbibition recovery of pore-fracture systems in tight oil reservoirs. Cai (2021) counted the number of papers and citations on imbibition over the past 20 years. In general, these studies have the characteristics of broad coverage, multiple research methods, and wide research angles

(Ashraf and Phirani, 2019; Lyu et al., 2019; Bakhshian et al., 2020).

The theoretical analysis method mainly comprises the derivation of an imbibition scale model. There are usually four types of classical imbibition mathematical models. The Lucas-Washburn (Lucas, 1918; Washburn, 1921) model describes the flow in a single circular section capillary. The Aronofsky (1954) imbibition model provides an empirical model for the cumulative imbibition displacement amount and time. Handy's (1960) model characterizes the weight or volume of intruded water as proportional to the square root of imbibition time. Finally, the matrix-fracture channeling equation is more suitable for the actual reservoir simulation (Kazemi and Merrill, 1979). Furthermore, Hu and Guo (1998) studied the microscopic mechanism of water spontaneous imbibition displacement in low-permeability reservoirs by using the ideal variable diameter capillary and mathematical analysis methods. Standnes (2009) corrected the dimensionless time in the formula of the scale model of oil-water two-phase spontaneous imbibition to predict the recovery curve. Cai et al. (2013) proposed that the fractal geometry method could improve the imbibition mechanism criterion of fractured dual media and established a new fractal criterion model of the reciprocal Bond number formula.

In terms of physical experiments, Haugen et al. (2015) experimentally studied the influence of fluid viscosity and relative permeability on imbibition recovery, and demonstrated that both had a strong enhancing impact. An experimental method for the quantification of spontaneous imbibition in geologic materials has also been proposed (Zahasky et al., 2019), which makes it possible to perform spontaneous imbibition experiments under high-pressure conditions. Wang et al. (2022) conducted an imbibition experiment in a modified LW model, determined the Tolman length, and added fluid-to-wall friction to the resistance term in the equilibrium force equation. With the development of science and technology, Computed Tomography and nuclear magnetic resonance techniques have also been implemented to study fluids in porous media (Liang et al., 2021). Imbibition experiments on tight oil reservoir cores were carried out in all of the relevant studies, and the study variables included the pore characteristics and boundary conditions of the core, and the salinity and mineral composition of fluids (Mason and Morrow, 2013). These studies focused on the improved oil displacement efficiency value of imbibition.

Many numerical simulation methods have been developed to analyze pore-scale fluid flow in porous media, such as the pore network model (Blunt et al., 2002), smooth particle method (Tartakovsky and Meakin, 2006), level set method (Amiri and Hamouda, 2013), phase field method (Wang et al., 2015), among other methods. Compared to macro-scale simulations, pore-scale simulations can not only provide detailed information on the fluid flow in pores and throats, but can also easily capture some important physical phenomena, such as the capillary valve effect or preferential flow paths (Xu et al., 2017). To study the capillary pressure dynamics of two-phase flow in tight sandstone, Cao et al. (2020) adopted the U-net training test set method to establish a digital core model based on manually modified gray threshold segmentation. Diao et al. (2020) studied the effects of pore throat tortuosity and mixed wettability on the spontaneous imbibition of natural heterogeneous porous media by using the newly developed quasi-three-dimensional color-gradient lattice Boltzmann model. Gong et al. (2021) proposed a new full dynamic pore network modeling platform, which can be used to study the pore scale under various two-phase flow conditions in fractures. In the above approaches, the focus of numerical simulation of displacement and imbibition is the change of oil-water interface, and the findings have extended implications for predictions of capillary trapping behavior in fractured media.

The above research results mainly come from theoretical deduction of static imbibition (Mogensen and Stenby, 1998) and physical simulation experiments involving the influencing factors of dynamic imbibition (Schechter et al., 1994; Yildiz et al., 2006, Xu et al., 2020). Static imbibition cannot deeply reflect the actual working condition of reservoir development; however, physical simulation experiments of dynamic imbibition have high cost. To address these issues, we design a microscopic numerical model to simulate the whole dynamics process of displacement and imbibition in tight oil reservoirs with a pore-fracture system.

2. Methodology

2.1 Phase field method

By coupling the Cahn-Hilliard equation (Feng et al., 2020) and Navier-Stokes (N-S) equation, the phase-field method can accurately describe the fluid flow while guaranteeing the conservation of mass in porous media. For complex porous media with uneven particle distribution or fractal characteristics, the phase-field method can solve the flow problem at the complex moving interface. To characterize the different phases and phase interfaces without directly tracking the interface changes of the two fluids, dimensionless phase field variables were introduced. The corresponding fluid properties of each phase field constant can be expressed as (Amiri and Hamouda, 2014; Zhu et al., 2020):

$$\begin{cases} \rho(\vartheta) = \dfrac{1+\vartheta}{2}\rho_w + \dfrac{1+\vartheta}{2}\rho_o \\ \mu(\vartheta) = \dfrac{1+\vartheta}{2}\mu_w + \dfrac{1+\vartheta}{2}\mu_o \end{cases} \tag{1}$$

where $\vartheta = -1$ represents the oil phase, $\vartheta = 1$ represents the water phase, and $-1 < \vartheta < 1$ represents the oil-water interface; $\rho(\vartheta)$ denotes the density of fluid near the oil-water interface, kg/m^3, ρ_w denotes the water density, kg/m^3; ρ_o denotes the oil density, kg/m^3; $\mu(\vartheta)$ stands for the viscosity of fluid near the oil-water interface, mPa·s, μ_w denotes the water viscosity, mPa·s; μ_o is the oil viscosity, mPa·s.

The Cahn-Hilliard equation refers to the convectional diffusion equation describing the separation of two-phase or multiphase fluids by constructing the interface mixing free energy with a constant phase field to control the interface shape change. The expression is as follows:
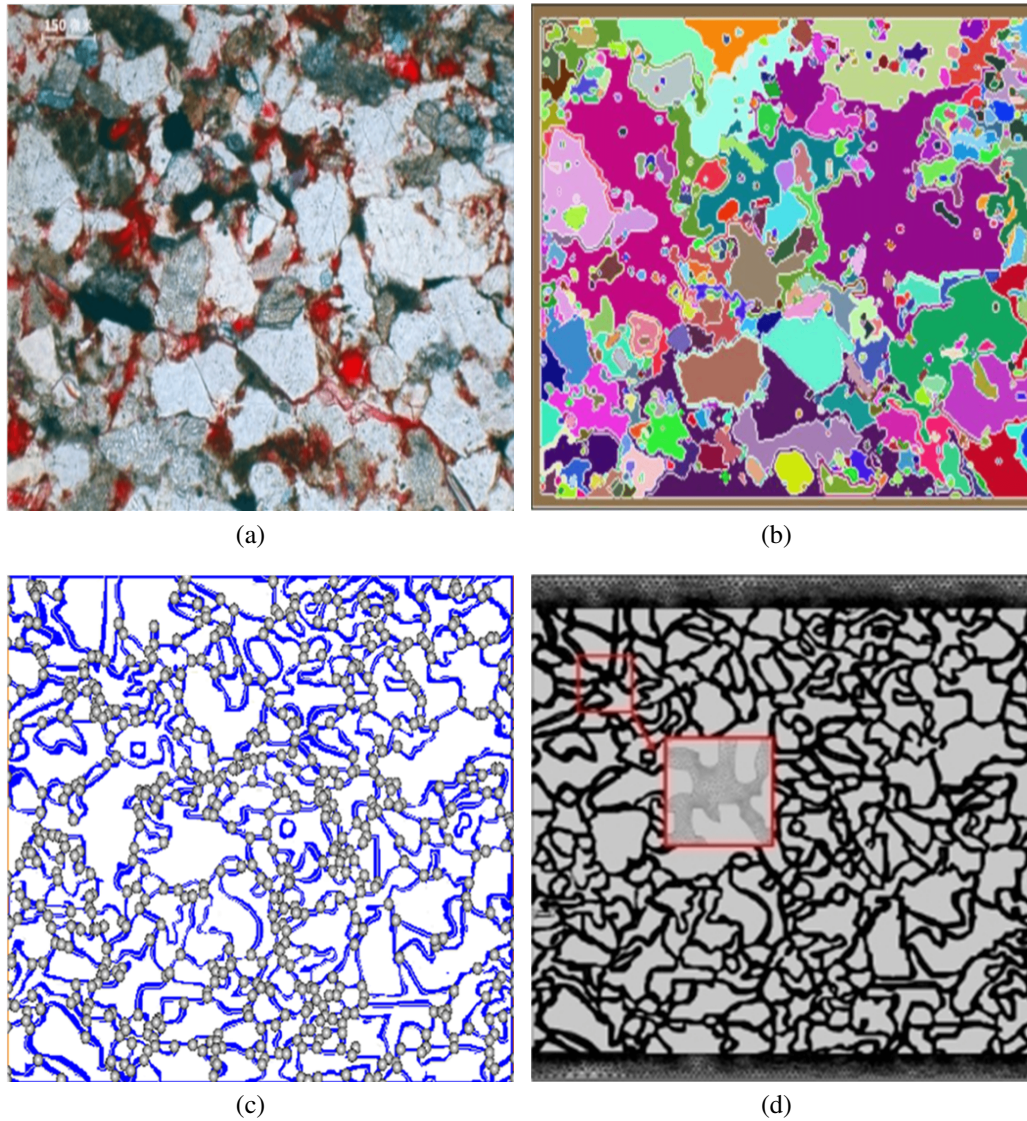
(a)   (b)

(c)   (d)

Fig. 1. Image recognition and processing: (a) core scanning image, (b) morphological processing, (c) pore and throat extraction and (d) grid division.

$$\begin{cases} \dfrac{\partial \vartheta}{\partial t} + u \cdot \nabla \vartheta = \dfrac{\gamma \lambda}{\varepsilon^2} \Delta \psi \\ \psi = -\varepsilon^2 \Delta \vartheta + \vartheta \left(\vartheta^2 - 1 \right) \end{cases} \quad (2)$$

where u represents the velocity of fluid, m/s; γ represents migration rate, m³·s/kg; λ represents mixed energy density, N; ε represents the thickness of interface, m; ψ is phase field auxiliary variable.

N-S equation: this is mainly used to describe the change in the mass and momentum of steady flow body. By introducing the interfacial tension as the mass force into the N-S equation, the flow process of the two-phase fluid is described as:

$$\begin{cases} \rho \dfrac{\partial u}{\partial t} + \rho u \cdot \nabla u = -\nabla pI + \nabla \cdot \left[\mu \left(\nabla u + \nabla u^T \right) \right] + F_{st} \\ \nabla \cdot u = 0 \end{cases} \quad (3)$$

where ρ denotes the fluid density, kg/m³; t denotes time, s; p is pressure, Pa; I is unit vector; μ denotes the fluid viscosity,

mPa·s; F_{st} denotes the interfacial tension, N/m.

2.2 Model establishment

This work presents a pore throat feature analysis method and a two-dimensional pore modeling method based on image recognition. Compared to the three-dimensional model, the two-dimensional model is preferred in pore-scale simulations for its advantage of low computational cost. The core casting thin section was sampled from well L134 in a block of the CQ Field. First, the actual core electron microscope scanning image Fig. 1(a) was grayscale processed. Then, morphological processing methods such as threshold segmentation, expansion corrosion, and manual modification methods were adopted to achieve edge smoothing and filter the additive noise of the image, in order to obtain the binarization image.

The pore and throat were extracted and analyzed based on the maximum spherical method and the central axis method,
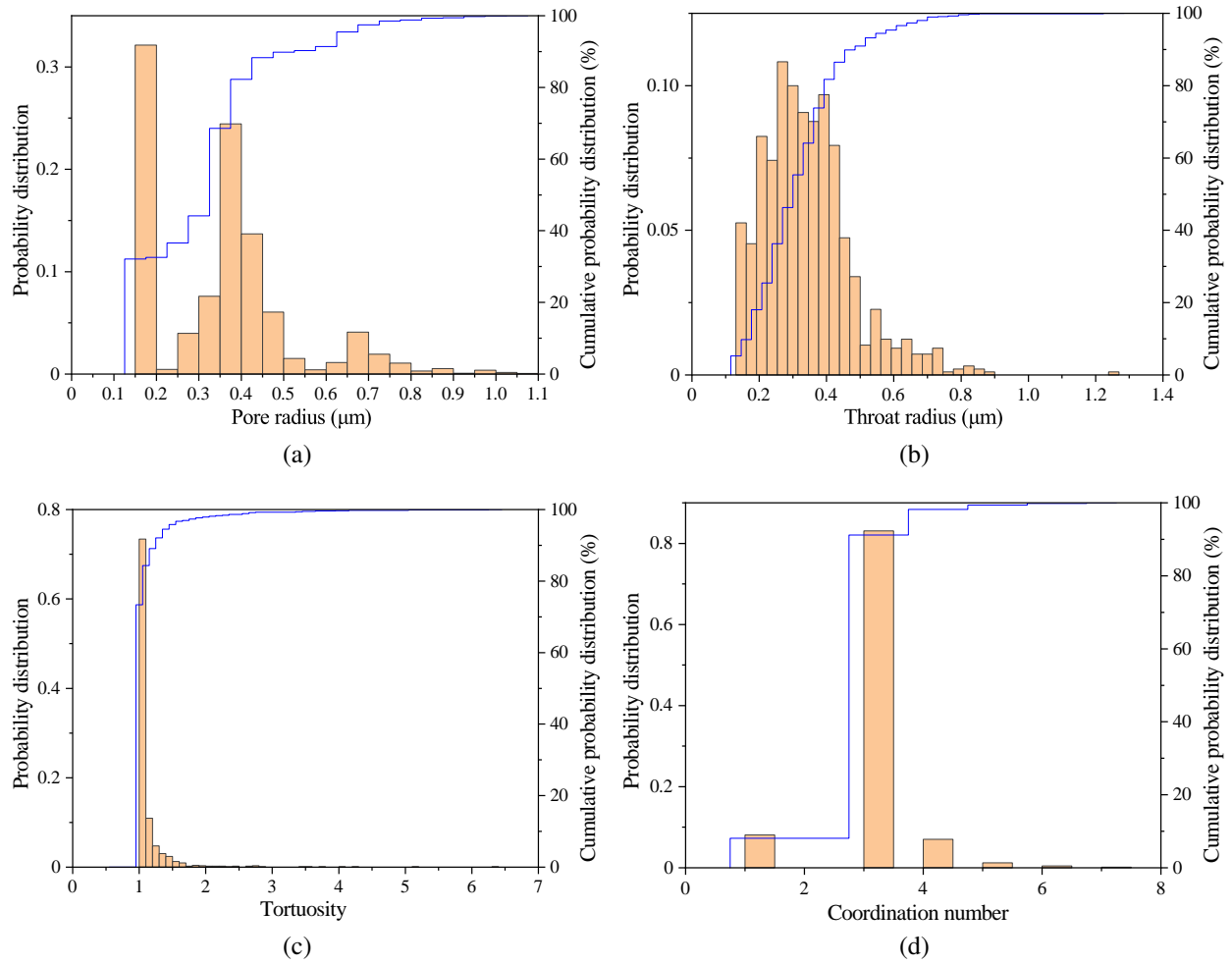
Fig. 2. The results of pore and throat characteristics analysis in the model: (a) pore characteristic, (b) throat characteristic, (c) tortuosity and (d) coordination number.

as shown in Fig. 1(c). To simulate the pore-fracture system, the upper and lower ends of the model were designed to simulate the fractures. Based on the binaryzation image, the AlgoLab Photo Vector was utilized for image vectorization and saved into CAD format (.dxf). Then, the CAD format file was imported into COMSOL Multiphysics software for grid division, and a total of 145,367 grids were divided, as shown in Fig. 1(d).

The results of pore characteristics analysis indicate unimodal distribution with different heterogeneity. The mean pore radius is about 0.35 μm, the mean throat radius is about 0.3 μm, the average tortuosity is 1.14, and the coordination number is 2.95, as shown in Fig. 2.

2.3 Program design and simulation process

The numerical simulation process is set as constant flow inlet and constant pressure outlet boundary, and the rest are non-flow boundary. The flow model adopts weakly compressible peristaltic flow and ignores the Stokes inertia and gravity terms.

Program 1: Inject water from the upper left end of the simulated fracture and produce oil from the lower right end.

Table 1. Main parameters of the displacement program.

parameter	Value
Model size (μm)	30×30
Viscosity of oil (mPa·s)	5
Viscosity of water (mPa·s)	1
Density of oil (kg/m^3)	850
Density of water (kg/m^3)	1,000
Surface tension coefficient (mN/m)	20
Interface thickness (μm)	0.5
Migration rate (m^3·s/kg)	1
Contact angle (rad)	$\pi/3$

The inlet boundary velocity is 50 μm/s and the outlet pressure is 1 atm. The oil-water interfacial tension is 20 mN/m, and the other parameters are shown in Table 1.

Program 2: During water displacement by the surfactant, the wettability of the formation core changes. Therefore, the contact angle of the microscopic model is adjusted from 60°
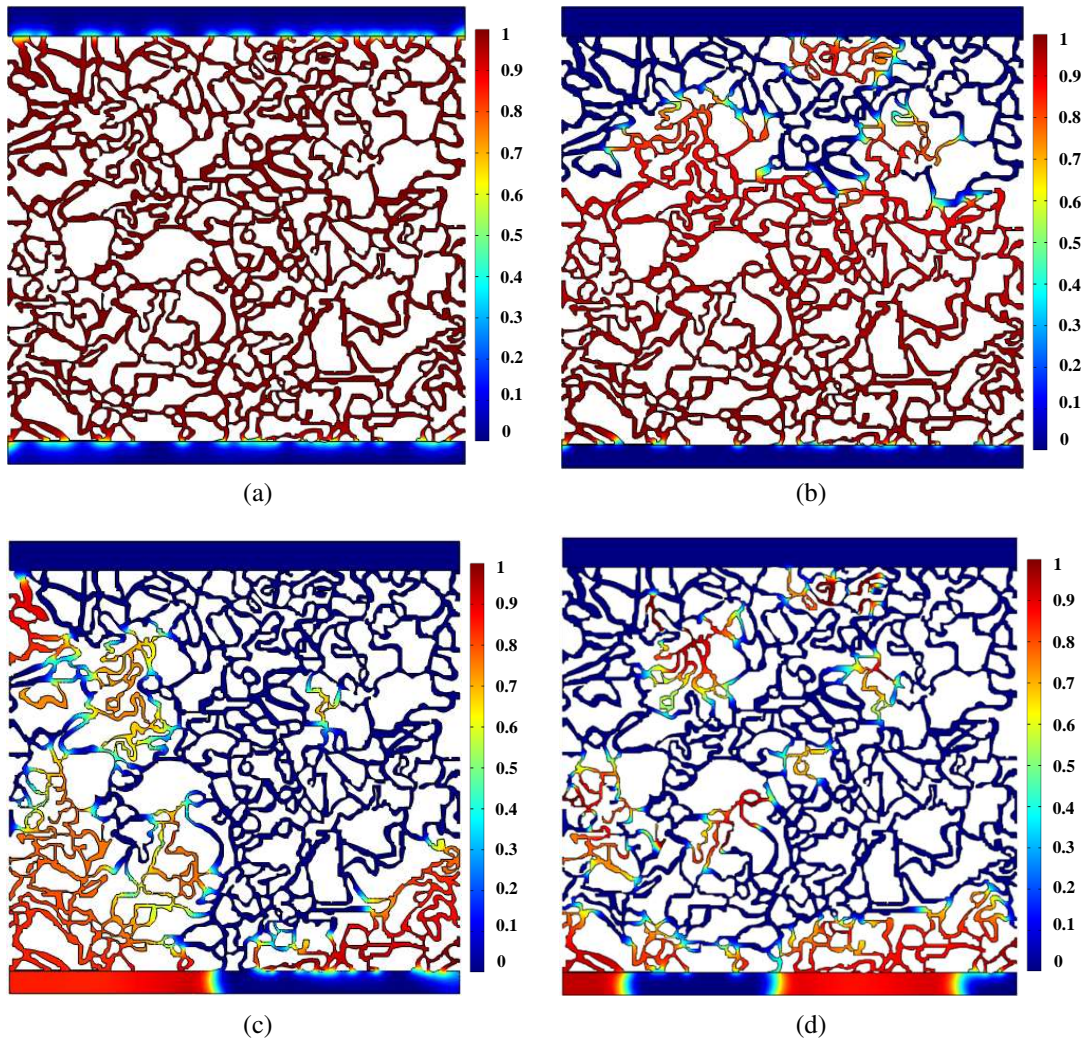
Fig. 3. Oil/water distribution of (a) initial condition and three injection programs: (b) displacement, (c) displacement by surfactant and (d) displacement-imbibition program.

to 30°, the oil-water surface tension coefficient is reduced, and other parameters remain unchanged.

Program 3: In the microscopic numerical model, the upper left end of the fracture is injected with water for 0~1 s at an injection rate of 75 μm/s. The injection rate gradually decreases for 1~3 s then comes to a stop, and the injection process resumes for 3~4 s. Oil is produced at the lower right end of the fracture, and the process of displacement and imbibition is simulated. All other parameters remain unchanged.

3. Results and discussion

Oil recovery in pore-fracture systems includes displacement and imbibition, while the flow characteristics of displacement and imbibition in tight oil reservoirs are extremely complicated. According to the direction of two-phase flow, imbibition can be divided into co-current imbibition and counter-current imbibition (Nooruddin and Blunt, 2016). Co-current imbibition refers to the process in which the flow direction of water is the same as that of oil, while the oil-water flow direction of countercurrent imbibition is exactly opposite to each other. According to the contact mode of the oil and water phase, imbibition can be divided into three types: unilateral contact imbibition, bilateral contact imbibition, and peripheral contact imbibition (Li et al., 2019). According to the spatial flow pattern, imbibition can be classified as plane imbibition and vertical imbibition, which will not be discussed here since the Bond number is relatively low and gravity is not considered.

Next, the water flooding process under the initial flow field condition is simulated, that is, the pore and throat fluids in the pore-fracture system are the oil phase, and the fluid in the fracture is the water phase, which simulates the bound water and fracturing fluid flowback. The oil and water distribution of three injection programs at the same time was obtained and shown in Fig. 3. The coupling mechanisms of displacement and imbibition with different injection media and injection methods in the two-dimensional microscopic numerical simulation model will be discussed in detail.
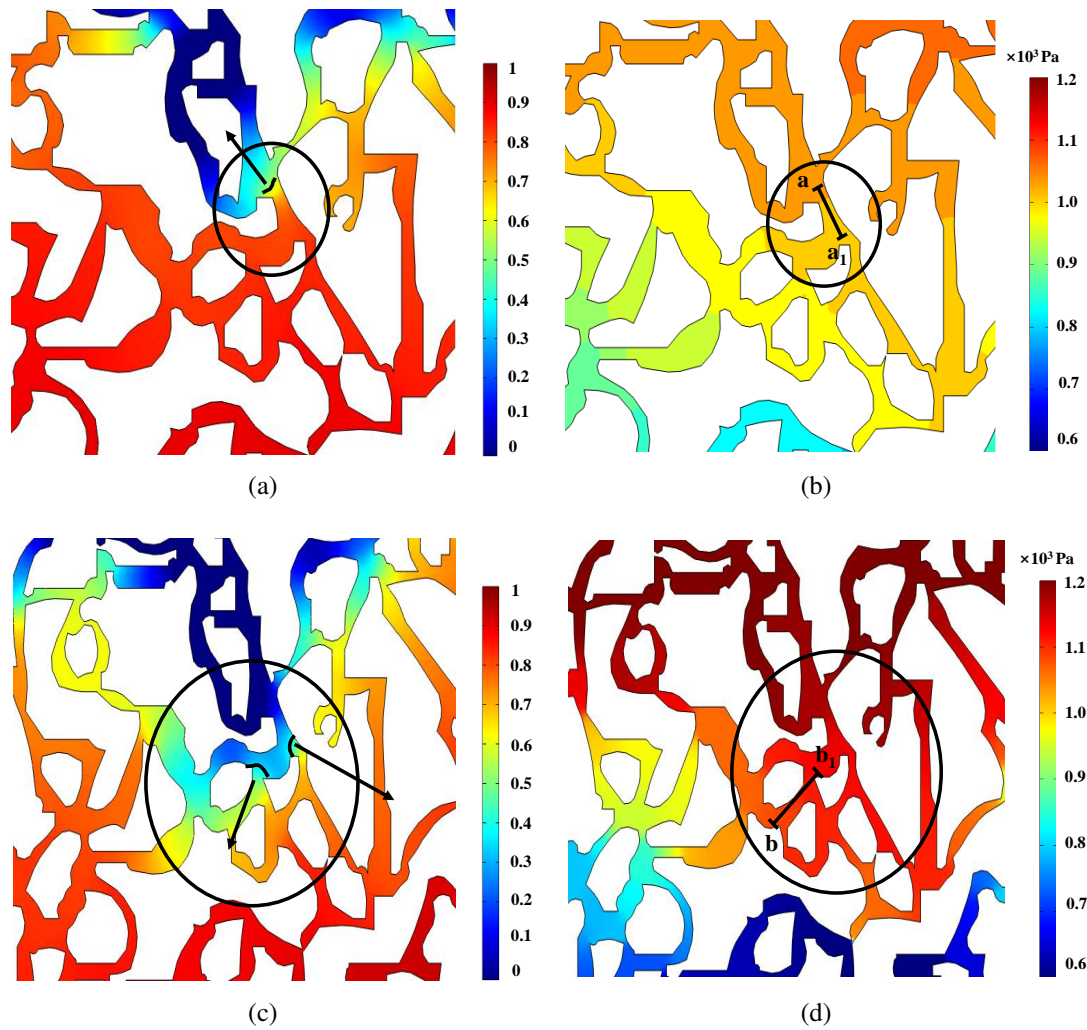
Fig. 4. Oil/water distribution and pressure distribution in the first research scope of different injection media: (a) oil/water distribution in the displacement program, (b) pressure distribution in the displacement program, (c) oil/water distribution in the displacement by surfactant program and (d) pressure distribution in the displacement by surfactant program.

3.1 Results and discussion

(1) Wettability changes

The same oil-water distribution range of two different injection media programs is selected as our research scope, as shown in Fig. 4. Under the displacement process, the original wettability of the model is middle wetting. When the radius of pore throat is small, the water injection velocity is large and the oil-water front interface is convex. Therefore, the capillary pressure represents the resistance of displacement. After adding the surfactant, the contact angle of the model becomes smaller and the oil-water interface becomes concave. The capillary pressure provides the driving force for oil recovery, resulting in two new flow paths. To further explain the causes of the imbibition phenomenon and eliminate the experimental contingency, the dynamic effects of imbibition recovery will be illustrated in combination with the numerical calculation of the pressure distribution of the model.

The displacement program is shown in Fig. 4(a) and Fig. 4(b). The pressure difference at the flow path aa_1 is 50 Pa, the contact angle in the middle-wet environment is close to 90°, and the capillary pressure is 0 Pa. After water injection by surfactant, the wettability changes and the fluid contact angle decreases, as shown in Fig. 4(c). The pressure difference at path bb_1 is about 100 Pa, and the capillary pressure obtained from the pore throat radius of 2 μm is about 100 Pa. Co-current imbibition promotes oil recovery, the combined force is 200 Pa, and the contribution of displacement and imbibition energy are both 50%. The pressure difference and capillary pressure calculation results of different flow paths are listed in Table 2.

(2) New flow paths appear

The flow direction of fluid in the displacement program is mainly transverse, as indicated in Fig. 5(a), with the cluster-remaining oil formed in the upper part of the matrix. After adding the surfactant, countercurrent imbibition occurs, and the water phase produces a new flow channel under the action of capillary pressure and enters the upper part. The upper remaining oil saturation decreases significantly.

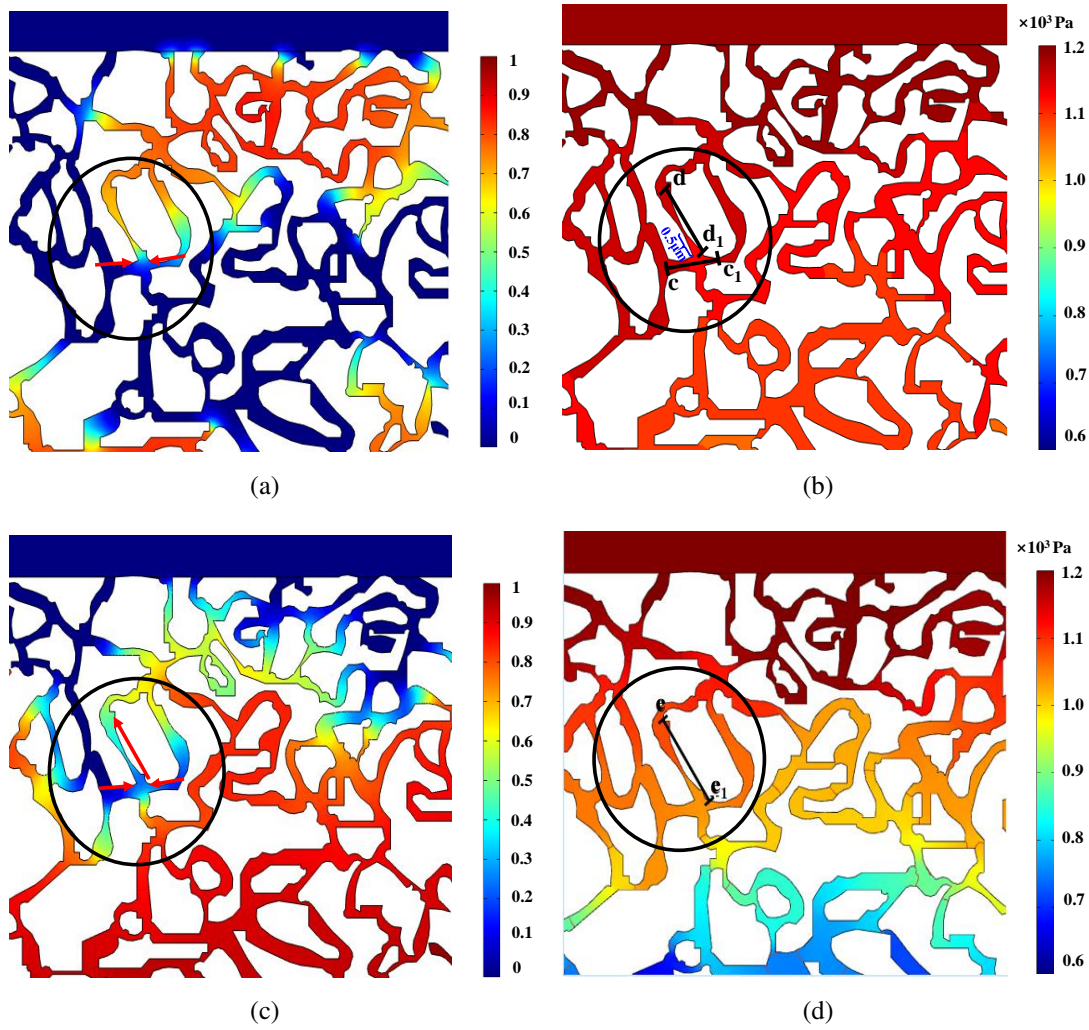In the displacement program, the water first flows along

Fig. 5. Oil/water distribution and pressure distribution in the second research scope of different injection media: (a) oil/water distribution in the displacement program, (b) pressure distribution in the displacement program, (c) oil/water distribution in the displacement by surfactant program and (d) pressure distribution in the displacement by surfactant program.

Table 2. Pressure difference and capillary force calculation results of different flow paths.

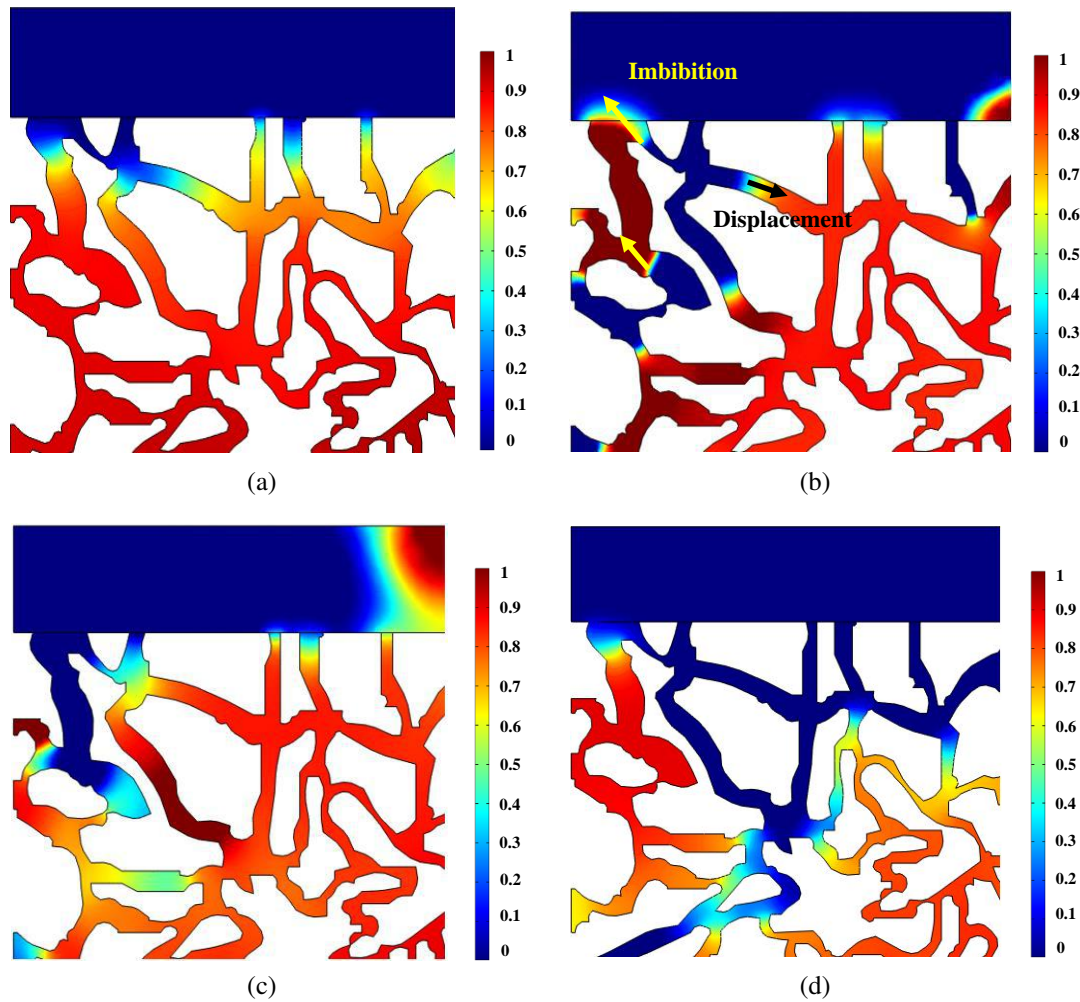| Flow path	Pressure difference (Pa)	Capillary force (Pa)	Combined force (Pa)	Energy contribution of pressure difference (%)	Energy contribution of capillary force (%)
aa_1	50	0	50	100	0
bb_1	100	100	200	50	50
cc_1	100	0	100	100	0
dd_1	100	0	100	100	0
ee_1	50	80	30	0	100
ff_1	500	400	100	100	0
gg_1	300	400	100	0	100

Fig. 6. Oil/water distribution in the full cycle production process during the displacement-imbibition program: (a) displacement stage, (b) the imbibition stage begins, (c) the imbibition stage ends and (d) production stage.

the transverse path cc_1 with a pressure difference of 100 Pa. At the bifurcation of the model, part of the fluid migrates upward. With the energy loss and insufficient power during the flow, the fluid is obstructed on path dd_1, and the action distance is only 0.5 μm. After adding the surfactant, the flow resistance inside the model is reduced. The pressure difference at path ee_1 is 50 Pa, as shown in Fig. 5(d). The capillary pressure is 80 Pa in a strong water-wet environment, which can overcome displacement pressure difference. The oil recovery by countercurrent imbibition capillary pressure excavates the remaining oil in the upper part and expands the affected area of water injection.

3.2 Different injection methods

In the displacement-imbibition program, the whole production cycle is revealed. Displacement stage: as shown in Fig. 6(a), water enters from the left end of the fracture and gradually occupies the capillary pore throat from top to bottom along the displacement direction. Injection termination and imbibition stage: in the early period, as shown in Fig. 6(b), the water phase occupies the central small pore throat under

the action of capillary pressure, and the oil phase discharges from the large pore throat and enters the fracture end; in the late period, as shown in Fig. 6(c), the oil droplets leave the pore throat completely and converge in the fracture. The oil production stage is shown in Fig. 6(d), and the oil phase in the fracture is reduced.

(1) Oil production action forms and positions

In view of the above model, the pressure distributions of the two programs are compared. The results show that the displacement process only has one flow direction from top to bottom, as shown in Fig. 7(a), that is, the oil production form is "displacement pressure difference". As illustrated in Fig. 7(c), there is another opposite flow direction, and the form of oil recovery in the displacement-imbibition program is "countercurrent imbibition and displacement".

There are differences in the location of oil and water when the two phases flow through the model. The results show that the displacement position is the large pore throat of the matrix due to its low friction resistance, and the countercurrent imbibition action position is the contact area between the matrix and fracture, as shown in Fig. 7(c). The water phase
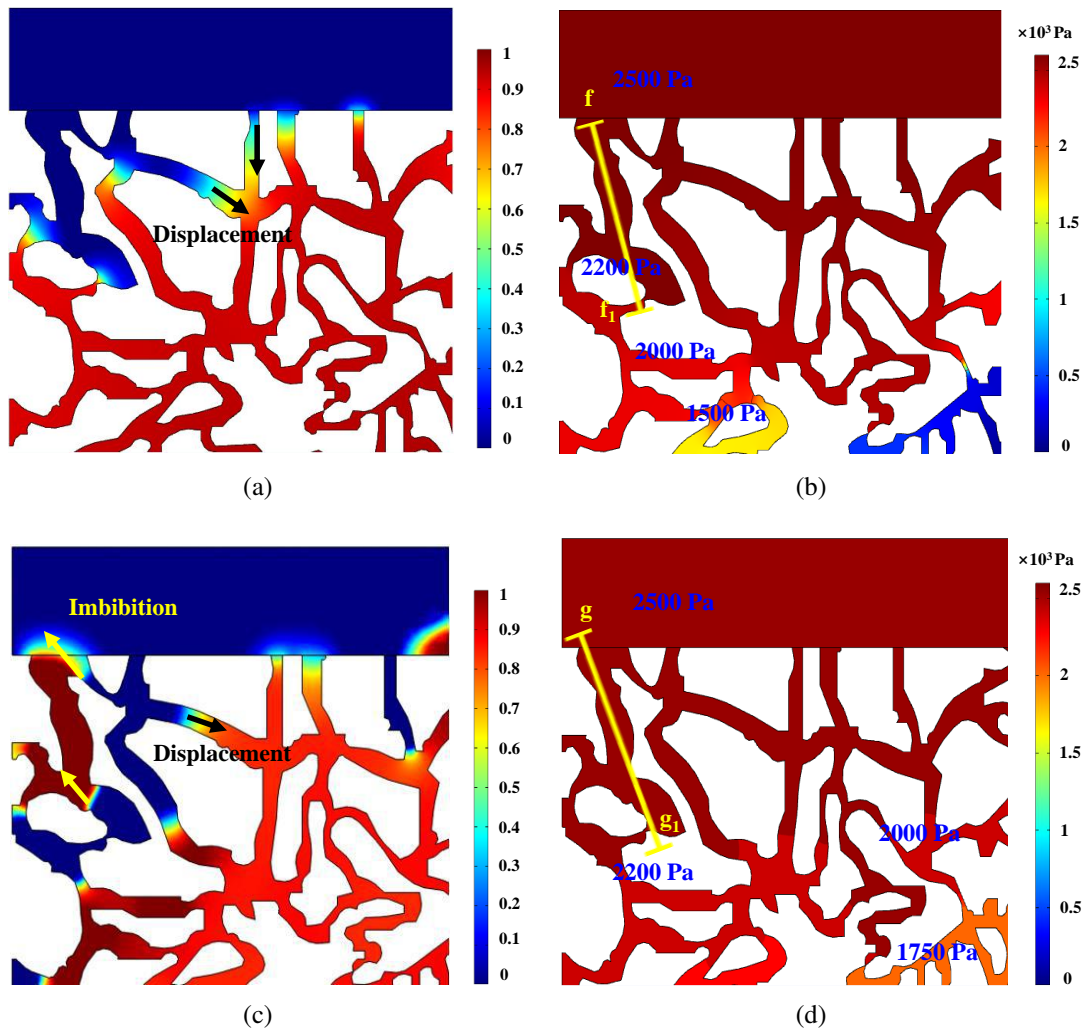
Fig. 7. Oil/water distribution and pressure distribution in the research scope of different injection methods: (a) oil/water distribution in the displacement program, (b) pressure distribution in the displacement program, (c) oil/water distribution in the displacement-imbibition program and (d) pressure distribution in the displacement-imbibition program.

occupies the matrix part, and the oil phase enters into the fracture after imbibition.

(2) Action conditions and pore limit

The nature of imbibition is largely determined by capillary pressure. Therefore, the co-current imbibition with the same direction of flow is performed under the condition of water-wet rock and moderate displacement rate, so that a concave surface can be formed. The condition of countercurrent imbibition opposite to the flow direction is that the capillary pressure is greater than the pressure difference. As can be seen in Fig. 7(b), the pressure difference of flow path ff_1 is 500 Pa in the displacement program. In the displacement-imbibition program, the displacement pressure difference of the flow path gg_1 at the same position is 300 Pa due to stopping the injection, which is less than that in the displacement program.

According to the calculation formula, the imbibition capillary pressure of the flow path bb_1 is 400 Pa, which is greater than the pressure difference of the displacement-imbibition program but smaller than that of the displacement program.

This means that countercurrent imbibition oil production by capillary force is inhibited in the displacement program. The maximum pressure difference of the displacement program is 500 Pa, and the corresponding conversion radius is 0.4 μm when it equals the capillary pressure. In other words, when the capillary pressure of pore throat with less than 0.4 μm radius is greater than 500 Pa, the countercurrent imbibition overcomes the difference in displacement pressure and will be the driving force of fluid flowing to the fracture. The energy contribution ratios of the displacement and imbibition are 0 and 100%, respectively.

In order to facilitate the investigation, several important and evident research scopes are selected, and then their oil saturation and pressure changes are analyzed. In fact, displacement imbibition is an objective existence and a joint action. Here, examples are given to demonstrate the existence of imbibition in other scopes. Due to space limitations, no more separate analysis and theoretical calculation will be involved.
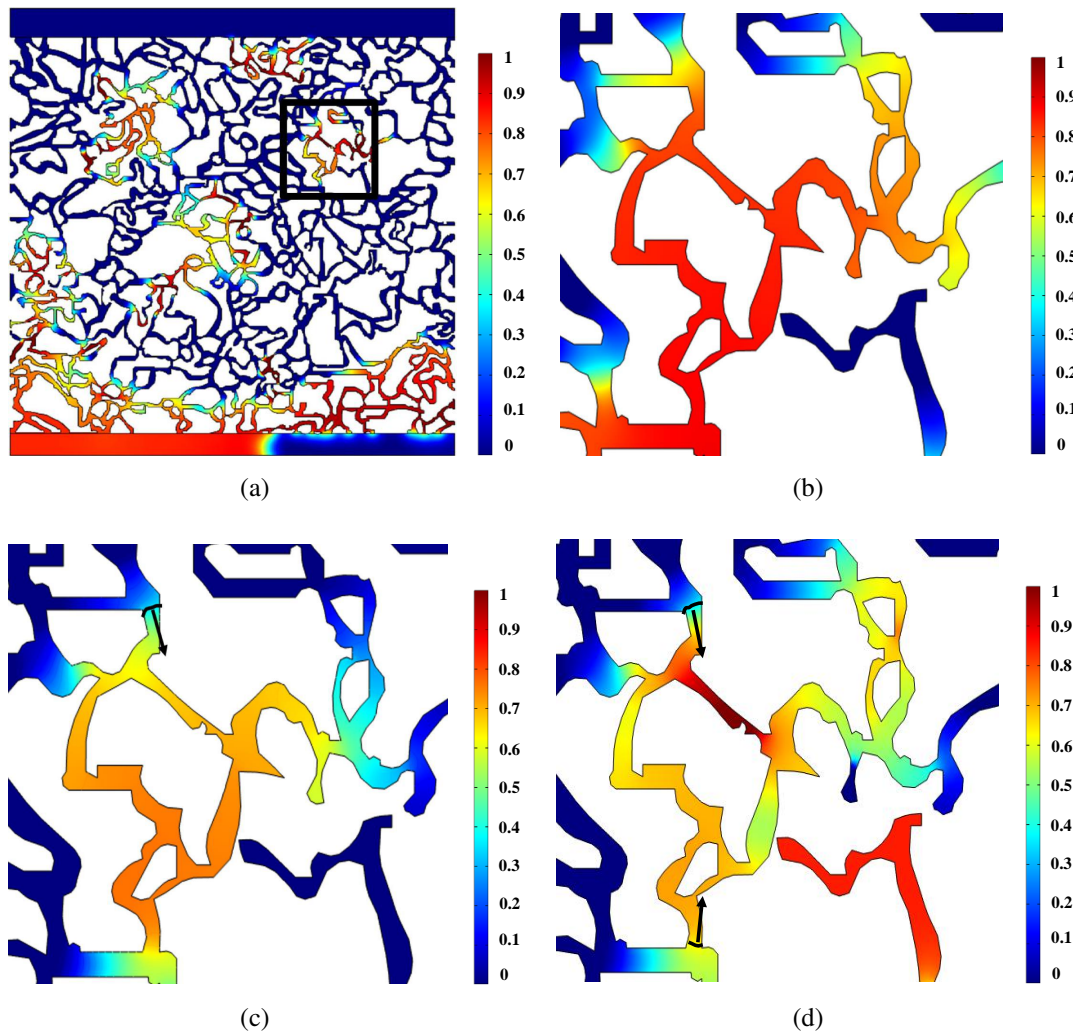
Fig. 8. (a) Select the research scope and and oil/water distribution of three injection programs at *t* = 2.76 s: (b) displacement, (c) displacement by surfactant and (d) displacement-imbibition program.

4. Conclusions

In this paper, the phase-field method in COMSOL Multiphysics software was used to simulate the oil-water two-phase flow, and a two-dimensional micro-model of the pore-fracture systems in tight oil reservoirs was established based on the pore throat characteristics. Then, the displacement imbibition recovery programs of different injection media and injection methods were carried out. The following conclusions could be drawn:

1) The effect of water injection with surfactant is changing the wettability of the model and promoting the capillary imbibition oil recovery. The direction of co-current imbibition is the same as that of displacement, which forms a coupling effect and increases oil production synergistically..

2) The main oil production form of the displacement program is pressure difference, and the large pore throat of the matrix is the first one to be used. Meanwhile, the action form of displacement-imbibition program is "coun-

tercurrent imbibition and displacement". The pressure difference distribution of pore throat is small in the stage of injection termination. The countercurrent imbibition overcomes the displacement pressure difference, replacing the oil in the matrix to the fracture and displacing it in the oil production period.

3) The acting condition of countercurrent imbibition opposite to the flow direction is that the capillary pressure is greater than the displacement pressure. In the pore-fracture system model designed in this paper, the maximum displacement pressure difference is 500 Pa in the research scope of displacement program, and the corresponding countercurrent imbibition opening pore throat size limit is 0.4 μm.

4) After the pore and fracture systems of tight oil reservoirs are formed by SRV, it is suggested to carry out the huff and puff measures to make full use of displacement imbibition combined energy and form a coupling effect. Surfactants can be injected appropriately to reduce the flow resistance and increase the contribution ratio of

production by imbition.

Acknowledgements

Conflict of interest

The authors declare no competing interest.

References

Abbasi, J., Ghaedi, M., Riazi, M. A new numerical approach for investigation of the effects of dynamic capillary pressure in imbition process. Journal of Petroleum Science and Engineering, 2018, 162: 44-54.

Abd, A. S., Elhafyan, E., Siddiqui, A. R., et al. A review of the phenomenon of counter-current spontaneous imbition: Analysis and data interpretation. Journal of Petroleum Science and Engineering, 2019, 180: 456-470.

Alava, M., Dubé, M., Rost, M. Imbition in disordered media. Advances in Physics, 2004, 53(2): 83-175.

Amiri, H. A., Hamouda, A. A. Evaluation of level set and phase field methods in modeling two phase flow with viscosity contrast through dual-permeability porous medium. International Journal of Multiphase Flow, 2013, 52: 22-34.

Amiri, H. A., Hamouda, A. A. Pore-scale modeling of non-isothermal two phase flow in 2D porous media: Influences of viscosity, capillarity, wettability and heterogeneity. International Journal of Multiphase Flow, 2014, 61:14-27.

Aronofsky, J. S., Jenkins, R. A simplified analysis of unsteady radial gas flow. Journal of Petroleum Technology, 1954, 6(7): 23-28.

Ashraf, S., Phirani, J. Capillary displacement of viscous liquids in a multi-layered porous medium. Soft Matter, 2019, 15(9): 2057-2070.

Bakhshian, S., Murakami, M., Hosseini, S. A., et al. Scaling of imbition front dynamics in heterogeneous porous media. Geophysical Research Letters, 2020, 47(14): e2020GL087914.

Blunt, M. J., Jackson, M. D., Piri, M., et al. Detailed physics, predictive capabilities and macroscopic consequences for pore-network models of multiphase flow. Advances in Water Resources, 2002, 25(8-12): 1069-1089.

Cai, J. Key problems and Reflections on spontaneous imbition of porous media. Chinese Journal of Computational Physics, 2021, 38(5): 505-512. (in Chinese)

Cai, J. Guo, S., You, L., et al. Fractal analysis of spontaneous imbition mechanism in fractured-porous dual media reservoir. Acta Physica Sinica, 2013, 62(1): 014701.

Cai, J., Jin, T., Kou, J., et al. Lucas-Washburn equation-based modeling of capillary-driven flow in porous systems. Langmuir 2021, 37(5), 1623-1636.

Cao, Y., Tang, M., Zhang, Q., et al. Dynamic capillary pressure analysis of tight sandstone based on digital rock model. Capillarity, 2020, 3(2): 28-35.

Diao, Z., Li, S., Liu, W., et al. Numerical study of the effect of tortuosity and mixed wettability on spontaneous imbition in heterogeneous porous media. Capillarity, 2021, 4(3): 50-62.

Feng, Q., Zhao, Y., Wang, S., et al. Pore-scale oil-water two-phase flow simulation based on phase field method. Chinese Journal of Computational Physics, 2020, 37(4): 439-447. (in Chinese)

Ghanbari, E., Dehghanpour, H. The fate of fracturing water: A field and simulation study. Fuel, 2016, 163, 282-294.

Gong, Y., Sedghi, M., Piri, M. Dynamic pore-scale modeling of residual trapping following imbition in a rough-walled fracture. Transport in Porous Media, 2021, 140(1), 143-179.

Habibi, A., Xu, M., Dehghanpour, H., et al. Understanding Rock-Fluid interactions in the montney tight oil play. Paper SPE 175924 Presented at SPE/CSUR Unconventional Resources Conference. Calgary, Alberta, 20-22 October, 2015.

Handy, L. L. Determination of effective capillary pressures for porous media from imbition data. Transactions of the AIME, 1960, 219(1): 75-80.

Haugen, Å., Fernø, M. A., Mason, G., et al. The effect of viscosity on relative permeabilities derived from spontaneous imbition tests. Transport Porous Media, 2015, 106, 383-404.

Hu, Y., Guo, H. Microscopic mechanism of imbition displacement in low permeability oilfield. Special Oil & Gas Reservoirs, 1998, 5(4): 18-22. (in Chinese)

Kazemi, H., Merrill, L. S. Numerical simulation of water imbition in fractured cores. Society of Petroleum Engineers Journal, 1979, 19(3): 175-182.

Li, C., Mao, W., Wu, T., et al. Study on the mechanism of imbition displacement. Xinjiang Petroleum Geology, 2019, 40(6): 687-694. (in Chinese)

Liang, Y., Lai, F., Dai, Y., et al. An experimental study of imbition process and fluid distribution in tight oil reservoir under different pressures and temperatures. Capillarity, 2021, 4(4):66-75.

Liu, J., Sheng, J. J. Investigation of countercurrent imbition in oil-wet tight cores using NMR technology. SPE Journal, 2020, 25(5): 2601-2614.

Lucas, R. Ueber das Zeitgesetz des kapillaren Aufstiegs von Flüssigkeiten. Kolloid-Zeitschrift, 1918, 23(1): 15-22.

Lyu, C., Ning, Z., Chen, M., et al. Experimental study of boundary condition effects on spontaneous imbition in tight sandstones. Fuel, 2019, 235: 374-383.

Mason, G., Morrow, N. R. Developments in spontaneous imbition and possibilities for future work. Journal of

Petroleum Science and Engineering, 2013, 110, 268-293.

Meng, Q., Cai, J., Wang, J. Scaling of countercurrent imbibition in 2D matrix blocks with different boundary conditions. SPE Journal, 2019, 24(3): 1179-1191.

Mogensen, K., Stenby, E. H. A dynamic two-phase pore-scale model of imbibition. Transport in Porous Media, 1998, 32, 299-327.

Nooruddin, H. A., Blunt, M. J. Analytical and numerical investigations of spontaneous imbibition in porous media. Water Resources Research. 2016, 52 (9): 7284-7310.

Rose, W. Fluid-fluid interfaces in steady motion. Nature, 1961, 191: 242-243.

Schechter, D. S., Zhou, D., Orr, F. M. Low IFT drainage and imbibition. Journal of Petroleum Science and Engineering, 1994, 11(4): 283-300.

Standnes, D. C. Calculation of viscosity scaling groups for spontaneous imbibition of water using average diffusivity coefficients. Energy & Fuels, 2009, 23(4): 2149-2156.

Tartakovsky, A. M., Meakin, P. Pore scale modeling of immiscible and miscible flows using smoothed particle hydrodynamics. Advances in Water Resources, 2006, 29(10): 1464-1478.

Wang, S., Feng, Q., Dong, Y., et al. A dynamic pore-scale network model for two-phase imbibition. Journal of Natural Gas Science and Engineering, 2015, 26: 118-129.

Wang, J., Salama, A., Kou, J. Experimental and numerical analysis of imbibition processes in a corrugated capillary tube. Capillarity, 2022, 5(5):83-90.

Washburn, E. W. The dynamics of capillary flow. Physical Review, 1921, 17(3): 273-283.

Xu, F., Chen, Q., Ma, M., et al. Displacement mechanism of polymeric surfactant in chemical cold flooding for heavy oil based on microscopic visualization experiments. Advances in Geo-Energy Research, 2020, 4(1): 77-85.

Xu, Z., Liu, H., Valocchi, A. J. Lattice Boltzmann simulation of immiscible two-phase flow with capillary valve effect in porous media. Water Resources Research, 2017, 53(5): 3770-3790.

Yildiz, H. O., Gokmen, M., Cesur, Y. Effect of shape factor, characteristic length, and boundary conditions on spontaneous imbibition. Journal of Petroleum Science and Engineering, 2006, 53(3-4): 158-170.

Zahasky, C., Benson, S. M. Spatial and temporal quantification of spontaneous imbibition. Geophysical Research Letters, 2019, 46(21): 11972-11982.

Zhou, X., Chen, D., Xia, Y., et al. Spontaneous imbibition characteristics and influencing factors of Chang 7 shale oil reservoirs in Longdong Area, Ordos Basin. Earth Science, 2022, 47(8): 3045-3055. (in Chinese)

Zhu, G., Yao, J., Zhang L., et al. Distribution and formation mechanism of remaining oil in ultra-high water cut period. Chinese Science Bulletin, 2017, 22(62): 2553-2564.

Zou, C., Yang, Z., He, D., et al. Theory, technology and prospects of conventional and unconventional natural gas. Petroleum Exploration and Development, 2018, 45(4): 604-618.